

## Retrieval of Ice Cloud Properties from AIRS and MODIS Observations Based on a Fast High-Spectral-Resolution Radiative Transfer Model

CHENXI WANG,\* PING YANG,\* STEVEN PLATNICK,+ ANDREW K. HEIDINGER,# BRYAN A. BAUM,@ THOMAS GREENWALD,@ ZHIBO ZHANG,& AND ROBERT E. HOLZ@

\* *Department of Atmospheric Sciences, Texas A&M University, College Station, Texas*

+ *Earth Sciences Division, NASA Goddard Space Flight Center, Greenbelt, Maryland*

# *NOAA/NESDIS/Center for Satellite Applications and Research, Madison, Wisconsin*

@ *Space Science and Engineering Center, University of Wisconsin—Madison, Madison, Wisconsin*

& *University of Maryland, Baltimore County, Baltimore, Maryland*

(Manuscript received 6 January 2012, in final form 10 August 2012)

### ABSTRACT

A computationally efficient high-spectral-resolution cloudy-sky radiative transfer model (HRTM) in the thermal infrared region ( $700\text{--}1300\text{ cm}^{-1}$ ,  $0.1\text{ cm}^{-1}$  spectral resolution) is advanced for simulating the upwelling radiance at the top of atmosphere and for retrieving cloud properties. A precomputed transmittance database is generated for simulating the absorption contributed by up to seven major atmospheric absorptive gases ( $\text{H}_2\text{O}$ ,  $\text{CO}_2$ ,  $\text{O}_3$ ,  $\text{O}_2$ ,  $\text{CH}_4$ ,  $\text{CO}$ , and  $\text{N}_2\text{O}$ ) by using a rigorous line-by-line radiative transfer model (LBLRTM). Both the line absorption of individual gases and continuum absorption are included in the database. A high-spectral-resolution ice particle bulk scattering properties database is employed to simulate the radiation transfer within a vertically nonisothermal ice cloud layer. Inherent to HRTM are sensor spectral response functions that couple with high-spectral-resolution measurements in the thermal infrared regions from instruments such as the Atmospheric Infrared Sounder (AIRS) and Infrared Atmospheric Sounding Interferometer. When compared with the LBLRTM and the discrete ordinates radiative transfer model (DISORT), the root-mean-square error of HRTM-simulated single-layer cloud brightness temperatures in the thermal infrared window region is generally smaller than 0.2 K. An ice cloud optical property retrieval scheme is developed using collocated AIRS and Moderate Resolution Imaging Spectroradiometer (MODIS) data. A retrieval method is proposed to take advantage of the high-spectral-resolution instrument. On the basis of the forward model and retrieval method, a case study is presented for the simultaneous retrieval of ice cloud optical thickness  $\tau$  and effective particle size  $D_{\text{eff}}$  that includes a cloud-top-altitude self-adjustment approach to improve consistency with simulations.

### 1. Introduction

Ice clouds, as a critical modulator of the radiation transfer between the earth's surface and the atmospheric system, play an important role in the Earth radiation budget through their albedo and greenhouse effects (Herman et al. 1980; Hartmann and Short 1980; Ohring and Clapp 1980; Stephens 2005; Eguchi et al. 2007). Currently, satellite-based remote sensing is the only viable means for obtaining global observations of ice cloud properties. However, the remote sensing of ice clouds is a challenging task because of their widely

varying horizontal and vertical distributions, formation-dissipation time scales, and the complicated morphology of nonspherical ice particles (Heymsfield and Iaquinta 2000; Heymsfield et al. 2002; Zhang et al. 2009). Satellite-based measurements provide an unparalleled opportunity for monitoring the global distribution of ice clouds and their optical and microphysical properties. In comparison with solar-reflectance-based retrieval algorithms (Nakajima and King 1990), the advantages offered by infrared (IR) sensors [e.g., the high-spectral-resolution sensors—the Atmospheric Infrared Sounder (AIRS; Aumann et al. 2003) and the Infrared Atmospheric Sounding Interferometer (IASI; Blumstein et al. 2004)] are that the ice cloud retrievals are consistent for both daytime and nighttime conditions and are less sensitive to ice particle habit, degree of surface roughness, and ice

Corresponding author address: Chenxi Wang, Dept. of Atmospheric Sciences, Texas A&M University, College Station, TX 77843.  
E-mail: chenx.wang@geos.tamu.edu

particle inhomogeneity. On the other hand, IR-based optical thickness retrievals are limited to lower values of optical thickness in comparison with solar reflectance-based techniques and require accurate surface temperature and atmospheric state profiles (e.g., Huang et al. 2004; Cooper and Garrett 2010). Some studies demonstrated that shortwave and IR observations provide complementary information and therefore the combination of the two can provide more consistent retrievals (Baran and Francis 2004).

To simulate the radiative transfer (RT) in a cloudy atmosphere, an accurate and rapid thermal IR radiative transfer model (RTM) that incorporates both gaseous absorption and multiple scattering within cloud layers is indispensable. The line-by-line (LBL) radiative transfer model (LBLRTM; Clough et al. 2005) is a rigorous approach that accounts fully for both the line absorption and continuum absorption (Clough et al. 1989) of various absorptive gases in the planetary atmosphere. However, the LBL model is too expensive computationally for consideration as an operational code where speed is a necessity. Many algorithms are available to alleviate the computing burden of the LBL model and include the Exponential Sum Fitting of Transmissions (ESFT; Wiscombe and Evans 1977; Armbruster and Fischer 1996), the correlated- $k$  distribution (CKD; Arking and Grossman 1972; Lacis et al. 1979; Goody et al. 1989; Lacis and Oinas 1991; Kratz 1995), the Optimal Spectral Sampling method (OSS; Moncet et al. 2008), the Principal Component-based Radiative Transfer Model (PCRTM; Liu et al. 2006), the Radiative Transfer for Television Infrared Observation Satellite (TIROS) Operational Vertical Sounder (RTTOV; Saunders et al. 1999, 2006), and the fast narrowband transmittance model (FFTM; Wei et al. 2007). These algorithms employ different theoretical approaches and are designed for different purposes. For example, the CKD and OSS methods simulate the spectral transmittance of a narrow interval by computing a selected number of representative monochromatic transmissions rather than fully considering the effects from the entire set of absorption lines, as is done in the LBL algorithm. The PCRTM removes the redundant monochromatic calculations using a principal component analysis and significantly improves the efficiency by the predetermined principal component scores. The FFTM uses precomputed nonlinear regression coefficients to fit the absorption coefficient with a moderate spectral resolution (i.e.,  $1 \text{ cm}^{-1}$ ).

In an absorptive-scattering medium, a cloud-scattering-property model is also a critical component in RT simulations. Various rigorous RTMs, such as the discrete ordinates radiative transfer model (DISORT; Stamnes et al. 1988) and the adding-doubling method (Twomey

et al. 1966; Hansen and Hovenier 1971), consider multiple scattering and are considered to be the standard benchmarks for RTMs. However, their high computation costs limit them from operational use in global cloud property retrievals from satellite sensors and global numerical weather prediction data assimilation efforts. To solve this problem, several previous studies (e.g., Baran and Francis 2004; Wei et al. 2004; Dubuisson et al. 2005; Heidinger et al. 2006; Wang et al. 2011) developed a series of fast RT equation (RTE) solvers to facilitate the design of ice cloud retrieval algorithms. In expanding from the single cloud layer to multilayered situation, Niu et al. (2007) developed a RTE solver to efficiently simulate upwelling radiance at the top of the atmosphere (TOA) for multilayered clouds. Based on the adding-doubling method, Zhang et al. (2007) developed a more flexible RTE solver that could be applied to multilayered clouds. A useful feature of this model is that it provides both upwelling radiance at the TOA and downwelling radiance at the surface and, thereby, benefits both space- and ground-based remote sensing applications.

In this study, a new high-spectral-resolution cloudy-sky radiative transfer model (HRTM) is developed to account for gas absorption. Specifically, a clear-sky transmittance database containing both line and continuum absorption is generated based on LBLRTM (version 11.7; Clough et al. 2005) with a  $0.1 \text{ cm}^{-1}$  spectral resolution. The total transmittance within a certain spectral interval of a thin inhomogeneous layer is determined by the absorber amount, density weighted pressure, and temperature. Based on this transmittance database, the layer absorption optical thickness is simulated. The model incorporates high-spectral-resolution ice cloud bulk scattering properties from Baum et al. (2007). The bulk scattering models were developed from ice crystal single-scattering properties (Yang et al. 2005; Zhang et al. 2004) and in situ ice cloud microphysical data, including both particle size distributions (PSDs) and particle habit distributions (HDs) (Heymsfield et al. 2002; Baum et al. 2005). The RTE solver (Wang et al. 2011) employed in the present study is made more efficient by using precomputed lookup tables (LUTs) of the transmittance, reflectance, effective emissivity, and effective temperature within an ice cloud layer to account for the multiple scattering, absorption, and thermal emission processes. Moreover, these ice cloud LUTs are updated for the high-spectral-resolution application. To apply the current forward radiative transfer model (i.e., HRTM) to infer ice cloud properties, such as cloud optical thickness  $\tau$  and effective particle size  $D_{\text{eff}}$ , a retrieval algorithm is developed that builds upon previous studies (Kahn et al. 2003; Huang et al. 2003; Huang et al. 2004; Kahn et al.

2004; Wei et al. 2004; Baran 2005; Li et al. 2004; Yue et al. 2007; Yue and Liou 2009). The main improvements of this algorithm are that 1) the HRTM-based method is computationally inexpensive so that it can be applied to operational global retrievals and 2) a cloud-top-altitude self-adjusting method is incorporated. The cloud altitude adjustment is typically 1 km, so that it is within the stated uncertainty of the height retrieval, but this is shown to be helpful in achieving better consistency with the inferred  $\tau$  and  $D_{\text{eff}}$  parameters.

The paper is organized as follows. Section 2 introduces basic principles of HRTM, including the clear-sky transmittance database and ice cloud LUTs. Section 3 evaluates the accuracy of model simulations in comparison with LBLRTM and DISORT. To improve our understanding of the ability of infrared-model-based retrievals, in section 4, we explore the sensitivity to the ice cloud properties of the brightness temperatures (BT) or the slope of the BTs across a wavenumber region. This section contains the description of an ice cloud retrieval algorithm and a case study. An error analysis is also included to explore the factors that impact the retrieved ice cloud properties. The summary and conclusions are given in section 5.

## 2. Forward model

The HRTM includes three components: 1) a fast clear-sky transmittance or absorption optical thickness simulator, 2) a fast RTE solver, and 3) an ice cloud multiple scattering–thermal emission and absorption model (Wang et al. 2011). This section describes the method and technical details related to the clear-sky gas absorption component of the HRTM.

For a given absorption line at an arbitrary monochromatic wavenumber, the absorption coefficient is mainly determined by pressure, temperature, and the spectral distance between the wavenumber and the center of the absorption line. However, for some strong absorbers, such as water vapor, the absorption coefficients are also influenced by the amount of substance present because of the self-broadening processes (Clough et al. 1989). For a clear atmospheric layer, the monochromatic transmittance depends on the absorption coefficient and the absorber amount. Instead of deriving clear-sky transmittance from the gas absorption coefficient as in LBLRTM, we build an extensive database of clear-sky transmittance as a function of pressure, temperature, and absorber amount. Based on this database, the monochromatic transmittance of the clear-sky layer can be derived efficiently and incorporated into an RTM under the plane-parallel cloud assumption.

In expanding from the single-layer case to a more complex atmosphere, the total monochromatic transmittance at a given wavenumber  $\nu$  is given by

$$T(\nu) = \prod_{i=1}^N T_i(\nu), \quad (1)$$

where the subscript  $i$  is the index of a homogeneous layer (i.e., constant pressure, temperature, and absorber amount). For practical use, a narrow spectral interval is defined such that the variation of the Planck function within the interval can be ignored, and the total spectral transmittance of the atmosphere within the interval approximately satisfies the multiplication in Eq. (1):

$$\bar{T}_{\nu} = \int_{\Delta\nu} \prod_{i=1}^N T_i(\nu) \frac{d\nu}{\Delta\nu} \cong \prod_{i=1}^N \int_{\Delta\nu} T_i(\nu) \frac{d\nu}{\Delta\nu}. \quad (2)$$

The spectral interval,  $0.1 \text{ cm}^{-1}$ , is found to satisfy the above conditions, while maintaining the simulation accuracy and the computational efficiency. For most simulations in the thermal IR window region ( $800\text{--}1200 \text{ cm}^{-1}$ ), the relative errors of the total spectral transmittances derived from the right side of Eq. (2) for clear-sky scenes are limited to 0.1% as compared with the accurate transmittances given by integrating Eq. (1) in the spectral intervals shown in Table 1. Note that we only consider the impact from the spectral interval on the simulation for narrowband instruments, such as the Moderate Resolution Imaging Spectroradiometer (MODIS), because a  $1 \text{ cm}^{-1}$  spectral interval is too large for the spectral response functions (SRF) of high-spectral-resolution instruments such as AIRS and IASI.

Simulations in the thermal IR region need to account for absorptive gases such as water vapor, carbon dioxide, carbon monoxide, ozone, methane, and nitrous oxide. The effect of continuum absorption due to the far wings of individual pressure broadening spectral lines is also important, especially in the  $700\text{--}1200$  and  $2000\text{--}3000 \text{ cm}^{-1}$  spectral regions (Clough et al. 1989). Several previous studies (e.g., Wei et al. 2007; Moncet et al. 2008) treat line absorption and continuum absorption separately; that is, the total transmittance of a layer is the product of the transmittances due to line absorption and those by the continuum absorption:

$$\bar{T}_{i,\nu} \cong T_{\text{cont}} \prod_{j=1}^M \bar{T}_{i,\nu}^j, \quad (3)$$

where the index  $j$  indicates the  $j$ th absorptive gas and  $T_{\text{cont}}$  is the transmittance contribution from continuum absorption. Similar to the case in Eq. (2), both the accuracy and computational efficiency of Eq. (3) decrease with the number of absorbers (Wei et al. 2007). In the HRTM, two steps are implemented to avoid a decrease

TABLE 1. Clear-sky layer transmittances calculated in different spectral resolutions.

MODIS IR band	0.001 cm <sup>-1</sup> spectral resolution	0.1 cm <sup>-1</sup> spectral resolution (relative error)	1.0 cm <sup>-1</sup> spectral resolution (relative error)
U.S. Standard Atmosphere			
Band 29 (8.5 μm)	0.7672	0.7680 (0.1%)	
Band 31 (11 μm)	0.8826	0.8822 (0.1%)	0.8638 (2.1%)
Band 32 (12 μm)	0.8348	0.8349 (0.0%)	0.8364 (0.2%)
Tropical summer profile			
Band 29 (8.5 μm)	0.5045	0.5052 (0.1%)	0.5041 (0.1%)
Band 31 (11 μm)	0.5192	0.5185 (0.1%)	0.4987 (3.9%)
Band 32 (12 μm)	0.4086	0.4087 (0.0%)	0.4093 (0.2%)

in both calculation speed and simulation accuracy due to multiple products. First, the contribution of continuum absorption is included in a precomputed transmittance database. Second, water vapor, carbon dioxide, and oxygen are treated as “mixed gases,” whose effective concentration is solely determined by the amount of molecular water vapor. The rationale is that carbon dioxide and oxygen can be considered to have a constant concentration in dry air, resulting in the amount of the mixed gas being solely determined by the water vapor content if the ambient pressure and temperature are specified. Additionally, water vapor and carbon dioxide are the two most important absorptive gaseous species throughout the IR region. As a result, the introduction of the mixed gas facilitates the model’s computational efficiency and the calculation accuracy of the continuum absorption resulting from water vapor self-broadening and foreign broadening. It is thus convenient to rewrite the thin-layer spectral transmittance [Eq. (3)], in the form

$$\begin{aligned} \bar{T}_{\Delta\nu, \text{total}} = & \bar{T}_{\Delta\nu}(P, t, u_{\text{mix}}) \times \bar{T}_{\Delta\nu}(P, t, u_{\text{O}_3}) \\ & \times \bar{T}_{\Delta\nu}(P, t, u_{\text{CO}}) \times \bar{T}_{\Delta\nu}(P, t, u_{\text{CH}_4}) \\ & \times \bar{T}_{\Delta\nu}(P, t, u_{\text{N}_2\text{O}}), \end{aligned} \quad (4)$$

where  $P$  and  $t$  are the pressure and temperature of a homogeneous clear-sky layer, respectively, and  $u$  is the gas amount within the layer.

The precomputed gas spectral transmittance database is generated using the latest version of LBLRTM

(version: 11.7; Clough et al. 2005) with the High-Resolution Transmission molecular absorption database (HITRAN 2004; Rothman et al. 2005), and including the Mlawer, Tobin, Clough, Kneizys, and Davies continuum model (also known as MT\_CKD v2.5; Mlawer et al. 2003). The spectral transmittances within the database are derived from integration of monochromatic transmittances computed by LBLRTM over a 0.1 cm<sup>-1</sup> interval. The spectral transmittances for each absorptive gaseous species are tabulated over hundreds of pressure levels, temperatures, and amount grids. To be more specific, the entire atmosphere is divided into three parts according to the pressure (i.e., low, median, and high). Table 2 gives the detailed information of the selected grids and of the spectral transmittances.

To apply the present database to simulate an arbitrary inhomogeneous thin clear-sky layer, the density-weighted effective layer pressure and temperature are used (Gallery et al. 1983). The definition can be expressed as follows:

$$\bar{P} = \frac{\int_{h_1}^{h_2} P(h)\rho(h) dh}{\int_{h_1}^{h_2} \rho(h) dh} \quad \text{and} \quad (5)$$

$$\bar{t} = \frac{\int_{h_1}^{h_2} t(h)\rho(h) dh}{\int_{h_1}^{h_2} \rho(h) dh}, \quad (6)$$

TABLE 2. The grids of precomputed transmittances.

Variables*	Low pressure layers	Median pressure layers	High pressure layers
Pressure (hPa)	50 grids: ~ (1150–100.0)	50 grids: ~ (100–10.0)	50 grids: ~ (10–0.1)
Temperature (K)	110 grids: ~ (309–200)	40 grids: ~ (239–200)	110 grids: ~ (309–200)
Absorber amount** (atm cm)	100 grids: ~ (10 <sup>-4</sup> –10 <sup>1</sup> )	100 grids: ~ (10 <sup>-4</sup> –10 <sup>1</sup> )	100 grids: ~ (10 <sup>-4</sup> –10 <sup>1</sup> )

\* Grid spacing of pressure and absorber amount is logarithmic.

\*\* The absorber amount of water vapor for lower part is from 10<sup>-4</sup> to 10<sup>3</sup> atm cm.

where  $h_1$  and  $h_2$  specify the lower and upper altitudes of a layer, respectively, and  $P(h)$  and  $\rho(h)$  indicate the pressure and density at altitude  $h$ . Subsequently, the layer spectral transmittance can be inferred from the database using three-dimensional interpolation. While the concentration of carbon dioxide has been increasing during the past 50 years, the  $\text{CO}_2$  concentration in the model is selected as 385 ppm without the seasonal variation. Were the model to be used for decadal satellite data processing, the changing concentration of  $\text{CO}_2$  would need to be considered.

A high-spectral-resolution bulk-scattering model for ice clouds (Baum et al. 2007) is employed in the model for calculating multiple scattering, absorption, and thermal emission processes within the ice cloud layer. Up to six habits of ice crystals (plates, droxtals, hollow columns, solid columns, 3D bullet rosettes, and hexagonal aggregates) are used for generating the database of single-scattering properties (Yang et al. 2005; Zhang et al. 2004). The ice cloud microphysical properties are calculated by assuming an HD as a function of particle size and a set of PSDs derived from in situ measurements in the midlatitudes, tropics, and subtropics (Heymsfield and Iaquinta 2000; Heymsfield et al. 2002). We neglect the potential vertical inhomogeneity in the ice cloud PSD and HD and only consider a linear variation of temperature within the layer. The IR optical thickness ( $\tau$ ) is referenced to the optical thickness at a visible wavelength (VIS,  $0.64 \mu\text{m}$ ).

The radiance simulations in an ice cloud layer consider multiple scattering, absorption, and thermal emission from the cloud. A 32-stream implementation of DISORT is used to calculate the angular-dependent ice cloud reflectance ( $R_c$ ), transmittance ( $T_c$ ), effective emissivity, and effective temperature functions. For an isothermal cloud layer, the effective emissivity ( $\varepsilon_{\text{eff}}$ ) is defined as the ratio of cloud boundary outgoing thermal emission ( $I$ ) to the blackbody radiance at temperature  $t$ :

$$\varepsilon_{\text{eff}}(v, \tau, D_{\text{eff}}, \mu) = \frac{I(t, v, \tau, D_{\text{eff}}, \mu)}{B(t, v)}, \quad (7)$$

where  $B$  is the Planck function and  $\mu$  indicates the cosine of the angle between the direction of outgoing radiance  $I$  and the normal direction of the cloud layer. For a nonisothermal cloud layer, the effective temperature ( $t_{\text{eff}}$ ) is defined as

$$t_{\text{eff}} = B^{-1}[I(t_{\text{top}}, t_{\text{base}}, v, \tau, D_{\text{eff}}, \mu)/\varepsilon_{\text{eff}}(v, \tau, D_{\text{eff}}, \mu)], \quad (8)$$

where  $B^{-1}$  is the inverse Planck function. The emitted radiance  $I$ , in this case, is also dependent upon the

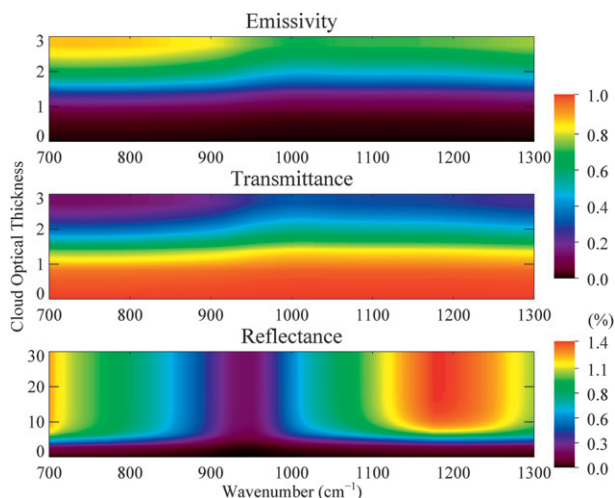


FIG. 1. Examples of precomputed LUT values (emissivity, transmittance, and reflectance) as a function of wavenumber and cloud optical thickness ( $D_{\text{eff}} = 50 \mu\text{m}$ ).

temperatures at the cloud-layer boundaries (i.e.,  $t_{\text{top}}$  and  $t_{\text{base}}$ ). The four parameters (i.e.,  $R_c$ ,  $T_c$ ,  $\varepsilon_{\text{eff}}$ , and  $t_{\text{eff}}$ ) defined are precomputed using the 32-stream DISORT for 33 VIS  $\tau$  values ranging from 0.01 to 100, 18  $D_{\text{eff}}$  values from 10 to  $180 \mu\text{m}$ , and nine viewing zenith angles from  $0^\circ$  to  $80^\circ$ . The LUTs for these parameters are generated at a  $0.1 \text{ cm}^{-1}$  spectral resolution from 700 to  $1300 \text{ cm}^{-1}$ . Figure 1 shows an example of the ice cloud LUTs. In the thermal IR window region, the ice cloud reflectance is close to 0 (especially near the  $950 \text{ cm}^{-1}$  region) due to significant absorption in the ice cloud. For this reason, higher-order reflections between the ice cloud layer and the surface can be safely ignored for simplification in this spectral region.

If the molecular scattering is ignored under clear-sky conditions as well as the higher-order reflected radiances between the ice cloud layer and the surface, the spectral TOA upward radiance (or BT) is composed of three parts (Wei et al. 2004): 1) the direct transmitted radiance from the thermal emission of the surface, the ice cloud, and the background atmosphere; 2) the first-order surface reflected radiance; and 3) the first-order ice cloud reflected radiance.

To work with satellite-based hyperspectral IR sensors such as AIRS and IASI, the TOA upwelling radiances are weighted by the SRF:

$$I_{\text{ch,TOA}} = \frac{\int_{\text{ch}} I_{\text{TOA}}(v) R_{\text{ch}}(v) dv}{\int_{\text{ch}} R_{\text{ch}}(v) dv}, \quad (9)$$

where  $R_{\text{ch}}(v)$  is the instrument SRF. For example, the AIRS sensor, consisting of 2378 IR channels, measures

the upwelling radiance at the TOA from 650 to 2670  $\text{cm}^{-1}$  with a spectral resolving power  $\nu/\Delta\nu = 1200$ . The half-width of the AIRS SRF increases moderately from 0.6 to 1.1  $\text{cm}^{-1}$  with increasing channel center wavenumber. To more accurately consider the AIRS SRFs, each SRF is truncated when the wavenumber distance is greater than 1.2  $\text{cm}^{-1}$  from the channel center. Therefore, Eq. (9) can be rewritten as

$$I_{\text{ch,TOA}} = \frac{\sum_{n=-12}^{12} I_{\text{TOA}}(\nu_{\text{ch}} + n\Delta\nu) R_{\text{ch}}(\nu_{\text{ch}} + n\Delta\nu)\Delta\nu}{\sum_{n=-12}^{12} R_{\text{ch}}(\nu_{\text{ch}} + n\Delta\nu)\Delta\nu}, \quad (10)$$

where  $\nu_{\text{ch}}$  is the center wavenumber of an AIRS channel and  $\Delta\nu$  is the spectral resolution of HRTM (i.e., 0.1  $\text{cm}^{-1}$ ).

### 3. Validation of the HRTM

In this section, the accuracy and efficiency of HRTM are evaluated by comparison with the benchmark models: LBLRTM+DISORT (hereinafter referred to as LBLDIS) for clear-sky cases (shown in Fig. 2) and cloudy-sky cases (shown in Fig. 3). Specifically, Fig. 2 shows the spectral transmittance as a function of wavenumber for a single inhomogeneous atmosphere layer with averaged pressure and temperature values of 975.0 hPa and 270.5 K, respectively [calculated from Eqs. (5) and (6)]. In the region between 800 and 1400  $\text{cm}^{-1}$ , the root-mean-square (RMS) transmittance difference between HRTM and LBLRTM is less than 0.001. For the cloudy-sky simulations, a midlatitude summer atmosphere is used. As shown in Fig. 3, the largest BT bias (HRTM – LBLDIS) of 0.2 K is found when an ice cloud is optically thin and consists of small particles. Meanwhile, relatively large RMS differences occur in the  $\text{CO}_2$  band (up to 0.25 K: 700–740  $\text{cm}^{-1}$ ) and the water vapor band (0.3 K: 1260–1300  $\text{cm}^{-1}$ ). One cause of the differences may be related to the strong absorption within the two bands, which may lead to significant transmittance variations and decrease the accuracy of applying the multiplication rule to HRTM with an assumed 0.1  $\text{cm}^{-1}$  spectral resolution. With a gradual increase in cloud optical thickness, the RMS error decreases from 0.2 to 0.1 K ( $\tau = 3.0$ ) to 0.05 K ( $\tau = 5.1$ ). For the last two cases, the TOA upwelling radiances are dominated by the ice cloud thermal emission as a result of the high optical thickness and ice particle absorption. An interesting point to note is that large departures in the BT spectrum can be found in the  $\text{CO}_2$  and  $\text{O}_3$  bands if a cloud layer is optically thick. This is caused by gas emission above the cloud layer that becomes significant if the background radiance is small

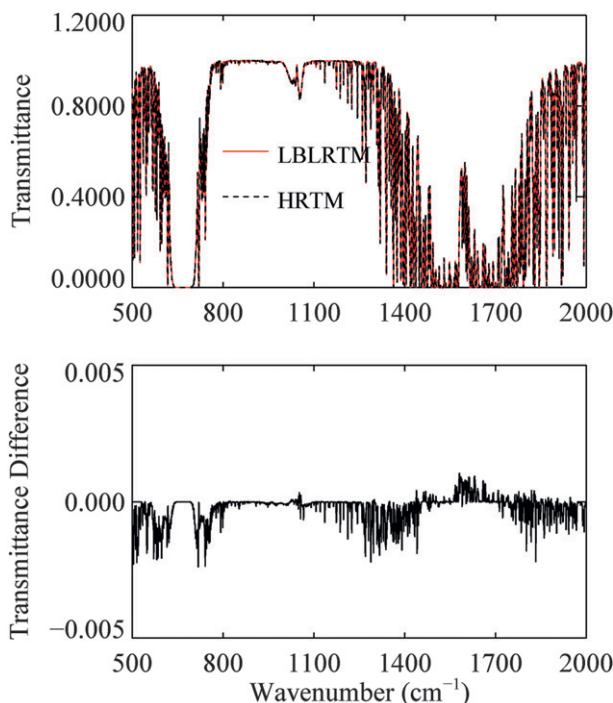


FIG. 2. Inhomogeneous clear-sky layer (top) transmittance derived by HRTM and LBLRTM and (bottom) transmittance difference;  $\text{H}_2\text{O}$ ,  $\text{CO}_2$ ,  $\text{O}_3$ , and  $\text{O}_2$  are considered. Averaged pressure and temperature are 975.0 hPa and 270.5 K, respectively.

(i.e., cloud is high in altitude and optically thick). Another special case is also included for validating the model capability for very thin cirrus cloud ( $\tau = 0.1$ ,  $D_{\text{eff}} = 10 \mu\text{m}$ ), which frequently occurs in the tropical tropopause layer (McFarquhar et al. 2000). In the thermal window region, the HRTM demonstrates an excellent ability to model this very thin cirrus cloud. With regard to the computational efficiency, HRTM simulates the TOA BTs (single ice cloud layer, 70 clear-sky layers, summer midlatitude profile) from 700 to 1300  $\text{cm}^{-1}$  at a 0.1  $\text{cm}^{-1}$  spectral resolution in a time that is three orders of magnitude faster than LBLDIS.

### 4. Retrieval of ice cloud properties using collocated MODIS and AIRS data

The ability of HRTM to rapidly and accurately simulate TOA BTs for cloudy-sky situations facilitates the inference of ice cloud optical and microphysical property retrievals. To illustrate the potential of the HRTM, an example is shown in this section using collocated imager (MODIS) and AIRS data. The AIRS L1B data are selected to provide the TOA upwelling radiances. To be more specific, 14 very narrow bands (DeSlover et al. 1999; Yue et al. 2007) are chosen between 800 and 1150  $\text{cm}^{-1}$  consisting of 152 AIRS channels (shown

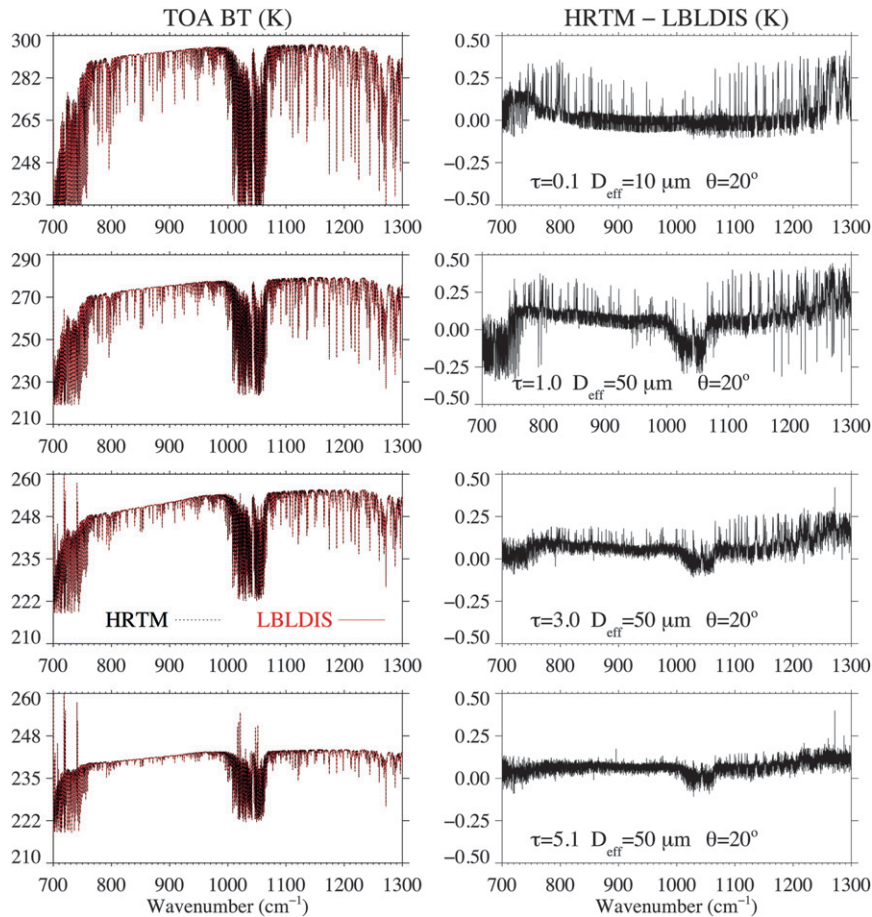


FIG. 3. (left) HRTM and LBLDIS (i.e., LBLRTM + DISORT) simulated TOA BTs and (right) their differences.

in Fig. 4) to conduct the inference of ice cloud properties. The bands are chosen for their sensitivity to ice cloud properties given the relatively weak gas absorption within the channels. The 152 AIRS channels are carefully chosen and display certifiable quality with similar calibration errors (the AIRS channel properties are available online: <http://disc.sci.gsfc.nasa.gov/AIRS/documentation>). In addition to AIRS L1B data, the *Aqua*/MODIS L2 cloud product (MYD06) provides the cloud-top pressure, and the MODIS operational Collection 5 (C5)  $\tau$  and  $D_{\text{eff}}$  retrievals derived from solar reflectance measurements at visible–near-infrared (VIS–NIR) and shortwave-infrared (SWIR) bands in MYD06 are extracted for comparison. The corresponding meteorological profiles are taken from the Modern-Era Retrospective Analysis for Research and Applications (MERRA; Rienecker et al. 2008) product.

#### a. Sensitivity study

The sensitivity of TOA BTs to ice cloud properties and geometric height is investigated for the case of a

midlatitude summer atmosphere with a single ice cloud layer. The surface is assumed to be a blackbody with a temperature of 299 K. Figure 5 demonstrates the sensitivities of TOA BTs to  $\tau$ ,  $D_{\text{eff}}$ , and cloud-top altitude. Several features are worth noting in Fig. 5. First, as expected, the TOA BTs are highly sensitive to  $\tau$ , especially in the cases of the optically thin and moderately thick ice clouds. TOA BTs decrease with an increase of  $\tau$  until they approach the cloud-top temperature. Second, the

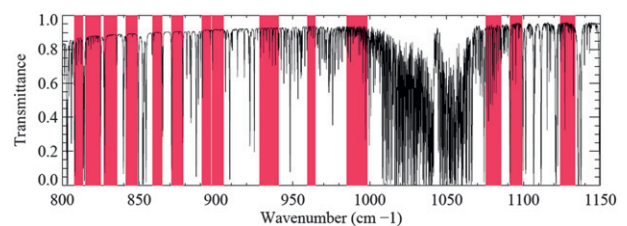


FIG. 4. Locations of the 14 narrow spectral bands (composed of 152 AIRS channels) selected for retrievals of ice cloud properties.

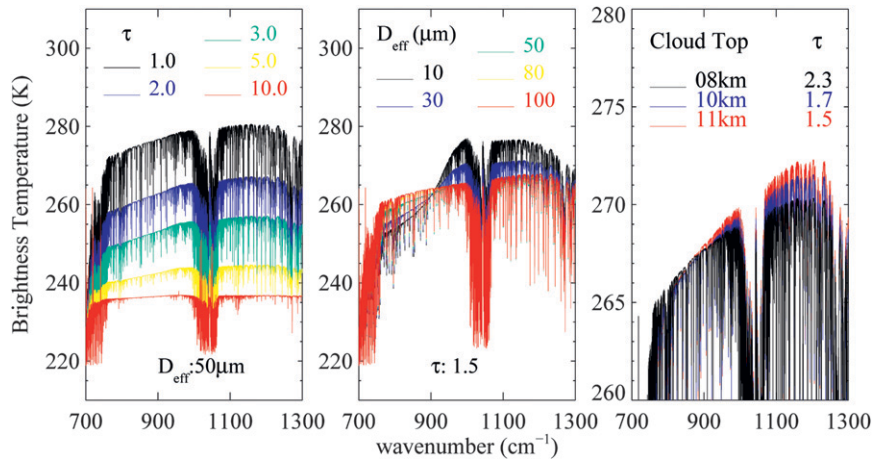


FIG. 5. Sensitivity of model-simulated TOA BTs to cloud optical thickness, effective particle size, and cloud-top altitude.

slope of the TOA BTs in the region between 800 and 960  $\text{cm}^{-1}$  is sensitive to  $D_{\text{eff}}$ , especially for ice clouds consisting of small ice particles. Note that the slope decreases rapidly once  $D_{\text{eff}}$  exceeds 80  $\mu\text{m}$  or the cloud becomes optically thick. Third, the BTs are also sensitive to cloud altitude. However, it is quite difficult to specify the cloud altitude through the comparison of measured to modeled BTs. The difficulty arises because the variation in BT driven by the change in cloud altitude has contributions from three main sources: the change in (a) the cloud internal temperature in the layer, (b) the transmitted thermal emission from the layers below the cloud, and (c) the gas absorption above the cloud. For example, shown in the right panel of Fig. 5, the model-simulated TOA BTs of a high-altitude, optically thin ice cloud ( $\tau = 1.5$ , cloud-top altitude = 11 km) can be quite similar to those derived from a lower-altitude but optically thicker ice cloud ( $\tau = 2.3$ , cloud-top altitude = 8 km) between 800 and 960  $\text{cm}^{-1}$ . The RMS BT difference between these two simulations in the 152 selected AIRS channels is less than 1 K. However, relatively large BTDs are found between 960 and 1150  $\text{cm}^{-1}$ . In this region, the absorption of ice particles is relatively weaker than in the region between 800 and 960  $\text{cm}^{-1}$ , and for the optically thin and higher clouds, more below cloud transmitted thermal emission and less above cloud gas absorption contribute to higher TOA BTs.

### b. Retrieval method

For each AIRS (or other high-resolution spectral resolution sensor) channel, the model simulation is primarily computed by the background atmospheric profile, cloud geometry, and ice cloud microphysical and

optical properties. To infer the optimal  $\tau$  and  $D_{\text{eff}}$  retrieval for a given cloud layer location, a least squares retrieval approach is defined similar to a previous study (Yue et al. 2007):

$$S(\tau, D_{\text{eff}}) = \sum_{i=1}^{152} (\text{BT}_{\text{Sim},i} - \text{BT}_{\text{Obs},i})^2, \quad (11)$$

where  $\text{BT}_{\text{Sim},i}$  and  $\text{BT}_{\text{Obs},i}$  indicate the model-simulated and AIRS-observed TOA BTs of the  $i$ th channel. Ideally, the cost function  $S$  approaches zero when  $\tau$  and  $D_{\text{eff}}$  are correctly specified. For this reason, the first objective of the retrieval is to find a  $\tau$ - $D_{\text{eff}}$  pair that minimizes  $S$ . To accommodate the information from the hyperspectral resolution instrument and to take advantage of the sensitivity of the BT slope (from 800 to 960  $\text{cm}^{-1}$ ) to the particle size for  $D_{\text{eff}}$  retrieval, the 152 AIRS channels are separated into two parts. The first part consists of the AIRS channels centered between 809 and 963  $\text{cm}^{-1}$  (100 channels), and the second part includes the AIRS channels located between 985 and 1135  $\text{cm}^{-1}$  (52 channels). The slope of the BTs in the first region (referred to as the BTS1) is computed to infer the cloud effective particle size (Huang et al. 2004; Wei et al. 2004). In the second region, the reasoning is as follows: if the average of the absolute values of the BTDs between the simulated and observed values (model – observation, referred to as the BTD2) is larger than 0.5 K, the cloud altitude is adjusted until better agreement is reached.

From an initially estimated  $\tau$  value (i.e., 3.0), a value of  $D_{\text{eff}}$  is derived from matching observed BTS1. Subsequently, based on this  $D_{\text{eff}}$  value, a refined  $\tau$  value is derived by minimizing the discrepancy between HRTM-simulated

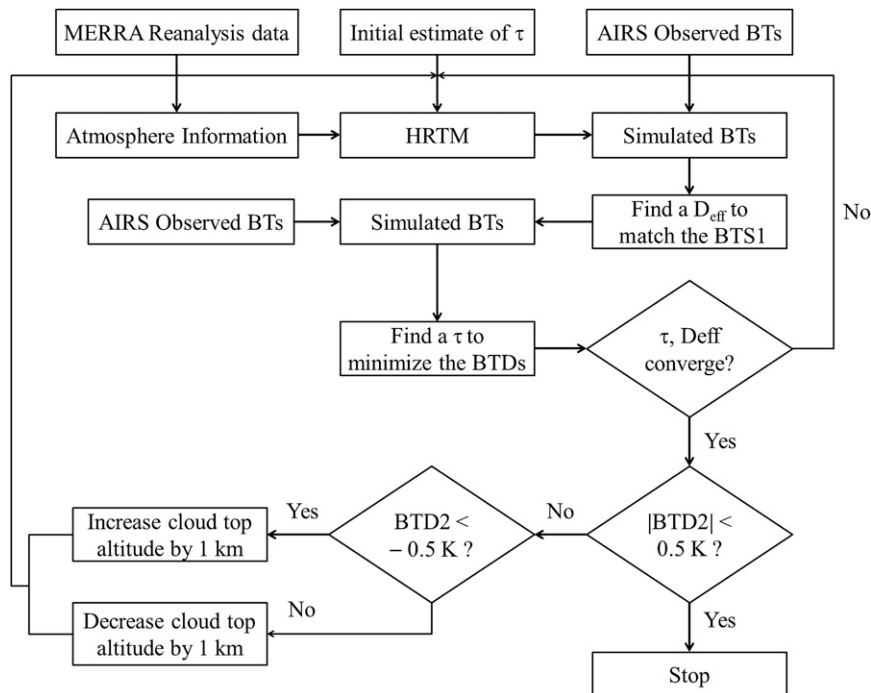


FIG. 6. Flowchart of the ice cloud retrieval algorithm. BTS1 indicates the BT slope in the region between 809 and 963  $\text{cm}^{-1}$ ; BTD2 indicates the average of absolute values of BT differences (simulation – observation) in the region between 985 and 1135  $\text{cm}^{-1}$ .

and AIRS-observed BTs. The retrieval program repeats these two steps until both  $\tau$  and  $D_{\text{eff}}$  converge. The program checks the BTD2 to determine whether a cloud-altitude adjustment is needed. The flowchart for the retrieval algorithm is illustrated in Fig. 6.

### c. Error analysis

As mentioned previously, the model uncertainties of ice cloud cases are generally within 0.2 K when compared with DISORT in the spectral region between 800 and 1150  $\text{cm}^{-1}$ . Therefore, the accuracy of the model-based retrieval is determined primarily by the uncertainties in the actual radiance measurements, ancillary data (temperature and water vapor profiles, surface temperature, etc.), and the cloud geometry (i.e., cloud layer geometric thickness and cloud-top altitude). We conduct an error analysis to evaluate the sensitivity of the retrieval algorithm to random errors by introducing  $\pm 1.0$  K, 1.0 K,  $\pm 100\%$ , 0.2 K, and  $-0.05$  random errors into the temperature profile, surface temperature, water vapor profile, AIRS BT observations, and surface emissivity, respectively. Furthermore, we also explore the impacts from cloud geometry on the retrieval of cloud properties. The midlatitude summer atmosphere mentioned in section 3 is employed to conduct this analysis. To avoid using cloud properties that exactly coincide with

those stored in the model LUTs, two sets of randomly selected cloud properties:  $\tau$  (0.53, 1.07, 1.69, 2.12, 3.02, 4.04, 5.16, 6.92, 9.90, and 12.03) and  $D_{\text{eff}}$  (20.38, 31.26, 39.74, 51.25, 72.36, 80.00, and 91.07  $\mu\text{m}$ ) are employed as reference values.

Figure 7 shows the relative errors of the retrievals that result from the introduction of the various sources of error. Generally, if the errors arise from the temperature profile and satellite measurement (i.e., Figs. 7a and 7c), the relative errors for ice cloud  $\tau$  retrieval are generally limited to 10% and increase with increasing reference  $\tau$ . However, the impacts from water vapor profile, surface temperature, and emissivity (i.e., Figs. 7g, 7e, and 7i) result in relatively large biases of  $\tau$  retrieval when clouds are optically thin. For example, a decrease in the surface emissivity reduces the upward radiance at the cloud base. If cloud is optically thin, this effect cannot be ignored, so the retrieval algorithm tends to select a smaller  $\tau$  value to match the observed TOA radiance. For ice cloud particle size retrievals, after the introduction of temperature profile and radiance–BT measurement errors, the accuracy of the  $D_{\text{eff}}$  retrieval decreases with both increasing reference  $\tau$  and  $D_{\text{eff}}$  (i.e., Figs. 7b and 7d), and the relative errors of  $D_{\text{eff}}$  exceed 30% if both  $\tau$  and  $D_{\text{eff}}$  are large ( $\tau > 9$  and  $D_{\text{eff}} > 80 \mu\text{m}$ ). Similar to the  $\tau$  retrieval, the errors from the water

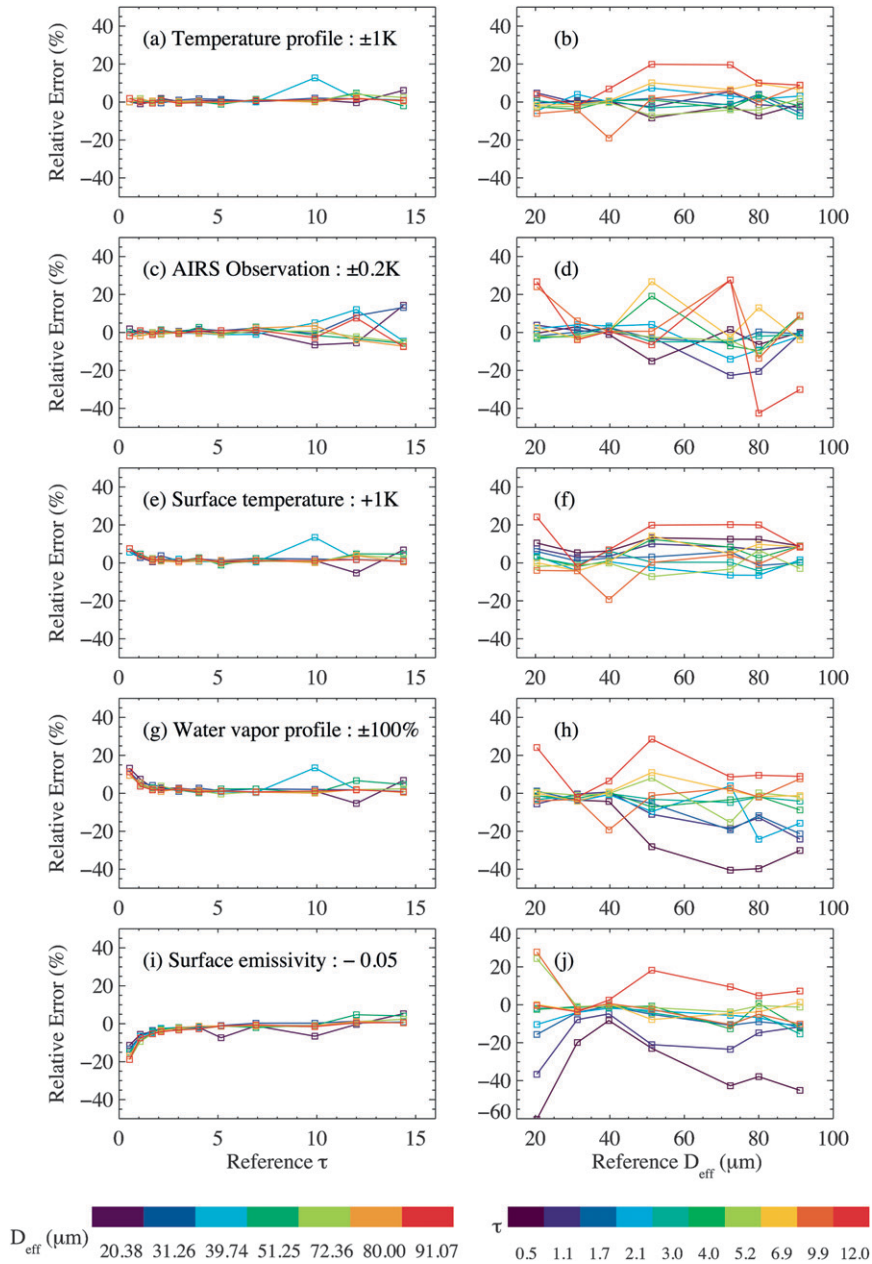


FIG. 7. Relative errors in (left) retrieved  $\tau$  and (right)  $D_{\text{eff}}$  caused by several error sources, i.e., (a),(b) temperature profile, (c),(d) AIRS observations, (e),(f) surface temperature, (g),(h) water vapor profile, and (i),(j) surface emissivity.

vapor profile, surface temperature, and emissivity significantly impact the inference of particle size if the cloud is optically thin (i.e., Figs. 7h, 7f, and 7j), suggesting that the impact from uncertainties from the surface and lower atmosphere (with high water vapor concentrations) on the retrieval can be offset by higher cloud opacity.

Figure 8 illustrates the influences from cloud-geometry errors on cloud retrievals. If the error comes from the

cloud-top altitude (the top two panels of Fig. 8), both the  $\tau$  and  $D_{\text{eff}}$  retrievals are reasonably stable because of the cloud-top altitude self-adjusting algorithm. The middle and bottom panels in Fig. 8 suggest that an inaccurate cloud physical thickness may cause systematic errors in the cloud property retrievals. Specifically, the overestimation of cloud physical thickness results in an overestimation of  $\tau$  and an underestimation of  $D_{\text{eff}}$ . Conversely, the underestimation of cloud physical

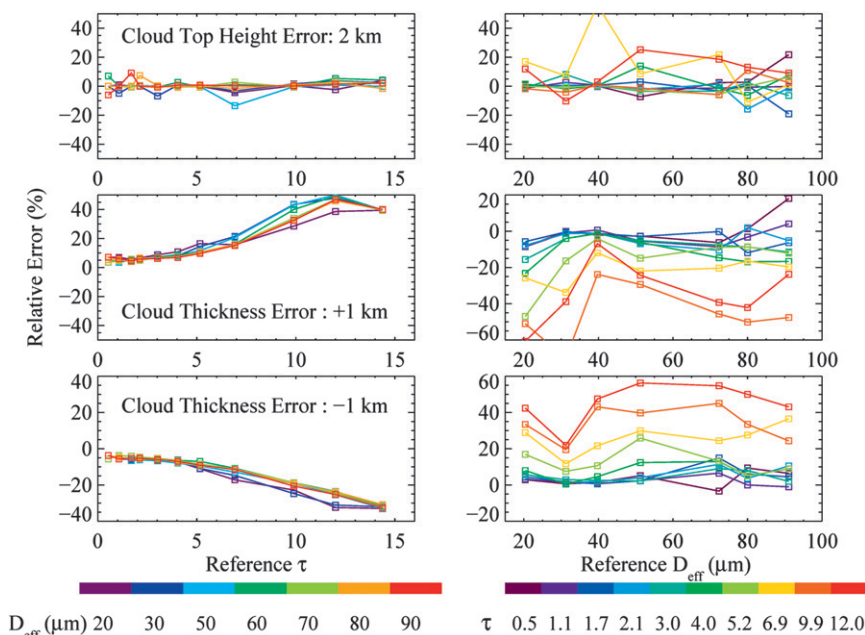


FIG. 8. As in Fig. 7, but caused by the cloud-top altitude and physical thickness.

thickness leads to an underestimation of  $\tau$  and an overestimation of  $D_{\text{eff}}$ .

Radiative transfer simulations show that the thermal IR radiances have limited sensitivity to optically thick cloud. We find the relative error of retrieved  $\tau$  to be quite small, however, if a reasonable error from the ancillary data or the TOA BT observations is introduced, even if the reference  $\tau$  exceeds 10. We are not suggesting that the IR-based retrieval (referred to as the IR retrieval) is reliable when cloud is optically thick. Some possible reasons for this are the following: 1) the error analysis gives us a general indication about the degree of impact on the cloud property retrieval from different error sources, and their variations with respect to both  $\tau$  and  $D_{\text{eff}}$ , and 2) the cloud inhomogeneity effects (both vertically and horizontally) are not taken into account in this study. The inhomogeneity effects can be significant. The IR retrievals are weighted toward the uppermost part of an optically thick cloud, suggesting that uncertainties in the retrievals may increase if the cloud is vertically inhomogeneous (e.g., Zhang et al. 2010). Therefore, we cannot simply conclude that the IR retrieval is accurate even if  $\tau$  is larger than 10 just based on the left panels in Fig. 7. Finally, the relative errors of retrieved  $D_{\text{eff}}$  values increase significantly for the optically thick cloud cases.

#### d. Case study

To illustrate the performance of the IR retrieval, the results are compared with the MODIS C5

operational products, which are based on VIS–NIR–SWIR measurements. The IR retrieval is applied to collocated data from the AIRS L1B and MODIS MYD06 products at 0045 UTC on 4 September 2007. AIRS has high spectral resolution but its field of view (FOV) is  $1.1^\circ$ , resulting in a lower spatial resolution of  $\sim 13.5$  km at nadir (Aumann et al. 2003), compared with the 1-km MODIS IR data. Thus, we degrade MODIS data to the resolution of an AIRS FOV following the collocation method suggested by Tobin et al. (2006). The AIRS FOV is assumed to be circular with its diameter increasing from 13.5 km at a subsatellite point to 35 km near the edge of the swath (see Fig. 9, left). An AIRS FOV is selected for retrieval if more than 90% of the MODIS pixels are marked as single ice cloud layer cases. For the present investigation, 120 collocated single-layer cirrus cloud cases are used; these are located in the region encompassed by the white box (around  $48^\circ\text{S}$ ,  $160^\circ\text{W}$ , over the southern Pacific Ocean) shown in the right panel of Fig. 9. The average MODIS C5 cloud-top pressures and surface temperatures in the selected AIRS FOVs are used in the retrievals. The sea surface is considered to be a Lambertian surface with a constant emissivity (0.98 is used in this study).

We first infer ice cloud optical thickness and cloud effective particle size based on AIRS TOA BT observations and the MODIS C5 cloud-top pressures. Subsequently, we compare the model-simulated TOA BTs based on the IR-retrieved cloud properties and those

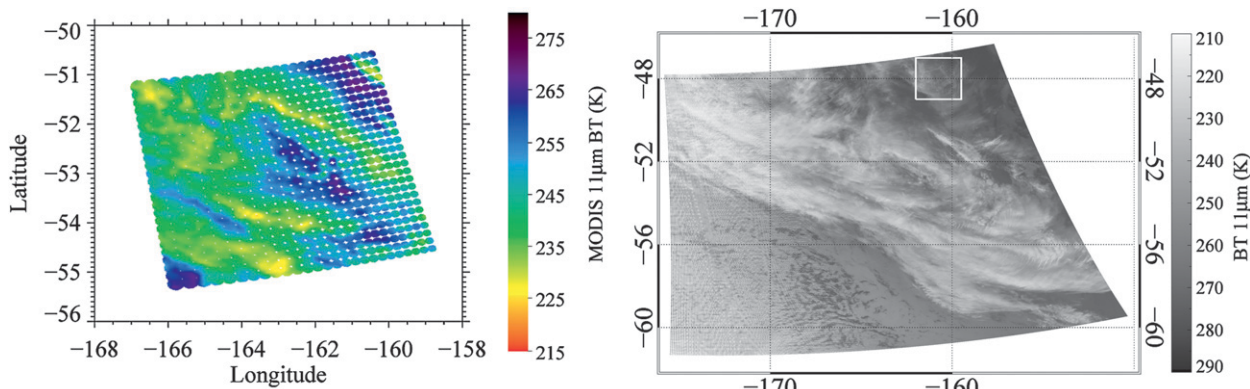


FIG. 9. (left) An example of the collocation of MODIS data (pixels) within AIRS FOVs (circles). The background is the MODIS band 31 ( $11\ \mu\text{m}$ ) BT. (right) MODIS band 31 ( $11\ \mu\text{m}$ ) BT image at 0045 UTC 4 Sep 2007. The collocated MODIS and AIRS data used in this case study are located in the white box (over the southern Pacific Ocean).

from AIRS observations. Figure 10 illustrates the corresponding comparisons of the BT values (left four panels) and BT spectrum images (right four panels) simulated by using retrieved cloud properties for several AIRS FOVs. In some cases, it is difficult to match BTS1 and minimize BTD2 at the same time. In reference to the right panel in Fig. 5, we believe the imbalance of the match of observed and simulated BTs before and beyond the ozone band may be caused by the uncertainty of the cloud altitude. To mitigate this problem, the cloud-top altitude in the MODIS C5 product is adjusted slightly. In this step, the value of BTD2 is considered to be a criterion for the altitude adjustment (see Fig. 6). Specifically, the cloud altitude is decreased by 1 km if BTD2 is larger than 0.5 K, whereas the altitude is increased by 1 km if BTD2 is smaller than  $-0.5$  K. Both the  $\pm 0.5$ -K threshold and the 1-km cloud-altitude adjustment are empirical according to dozens of simulations and retrieval tests. Further investigation is necessary to better understand the imbalance. The performance of this retrieval method is illustrated in Fig. 11. After a slight adjustment in cloud-top height, both the model-calculated BTS1 and BTs are in much closer agreement with their observed counterparts. The BT spectrum images simulated using two different retrieval results are shown in the right panels in Fig. 11.

Figure 12 shows the comparisons of retrieved cloud properties between MODIS C5 products and the present IR retrievals. Although the AIRS  $\tau$  values and their MODIS counterparts are well correlated (the correlation coefficient is 0.71), MODIS  $\tau$  values are systematically 2 times larger than the AIRS retrievals (the regression coefficient of AIRS  $\tau$  on MODIS  $\tau$  is 0.55; see Fig. 12a). Figures 12b and 12c demonstrate the comparisons of  $D_{\text{eff}}$  and cloud-top altitude values from MODIS C5 and the AIRS retrieval. In contrast to the

retrieval of  $\tau$ , the MODIS and AIRS  $D_{\text{eff}}$  values are relatively consistent. In comparing the MODIS C5 cloud-top heights with those adjusted by the AIRS retrieval, we find that within the 120 samples, the cloud-top heights of 72 cases are adjusted lower but only 22 are increased.

## 5. Summary and conclusions

The present study explores the development of a high-spectral-resolution radiative transfer model to rapidly and accurately simulate clear-sky transmittances for thin atmosphere layers. Compared with previous algorithms, the clear-sky simulations from this method (i.e., layer transmittance and absorption optical thickness) have inherent advantages for coupling with RTE solvers. To minimize the computational burden, a transmittance database is generated for seven major absorptive gases within the atmosphere at a  $0.1\ \text{cm}^{-1}$  spectral resolution, which is sufficient for considering the SRF of a spaceborne hyperspectral sensor. The layer transmittance of an individual absorber is completely determined by the absorber amount, density-weighted pressure, and temperature. Moreover, carbon dioxide and oxygen are treated as a mixed gas because of their relatively constant atmospheric concentrations. The effect of continuum absorption has been included in the present database to further reduce the computing time. For ice cloud simulations, a database (Baum et al. 2007) including MODIS C5 bulk-scattering properties is coupled with HRTM to consider the multiple scattering processes, absorption, and thermal emission within the ice cloud layer. Generally, the comparisons of clear-sky TOA BT simulations between HRTM and LBLRTM show differences of generally less than 0.05 K, except in the regions of the  $\text{CO}_2$  band (up to 3 K:  $700\text{--}740\ \text{cm}^{-1}$ )

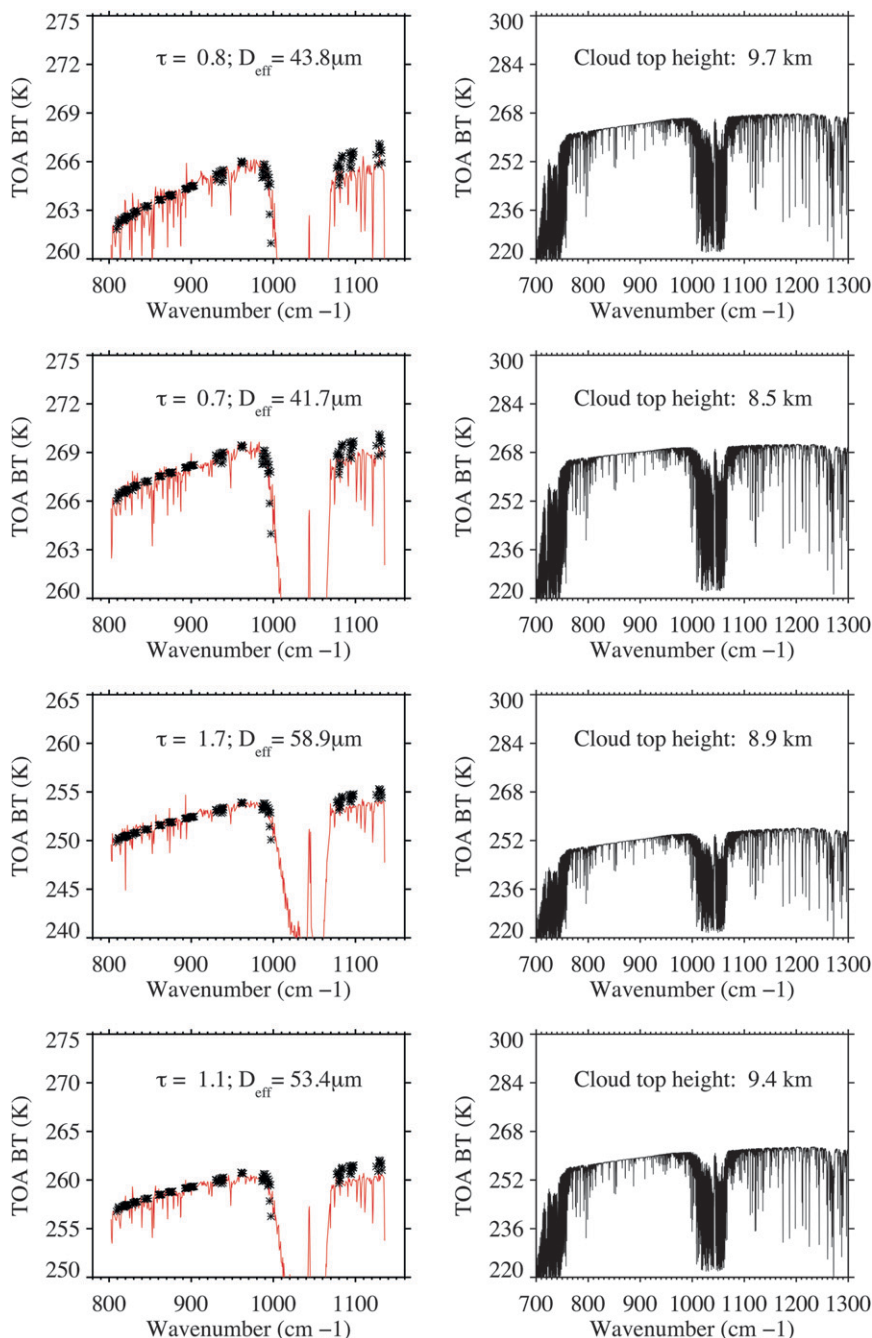


FIG. 10. (left) Model-simulated (black stars) TOA BTs vs AIRS observations (red curves), plotted by using four collocated pixels in the white box region in Fig. 9; the cloud properties are retrieved by minimizing the  $S$  function [see Eq. (11)] and using the MYD06 cloud-top pressure. (right) TOA BT spectrum images simulated by using the retrieved  $\tau$  and  $D_{\text{eff}}$  pairs.

and the water vapor band (0.2 K: 1260–1300 cm<sup>-1</sup>). For single ice cloud layer cases, the model simulation differences are generally limited to within 0.2 K. The computational speed of HRTM is three orders of magnitude faster than using LBLDIS. However, a limitation of HRTM is that the clear-sky transmittance database is

quite large (~20 GBytes). Additionally, this model can be applied only to cases that are clear sky or contain single-layer clouds.

A height-adjusting retrieval algorithm is presented based on HRTM and is applied to a case study using the collocated MODIS C5 products and AIRS L1B TOA

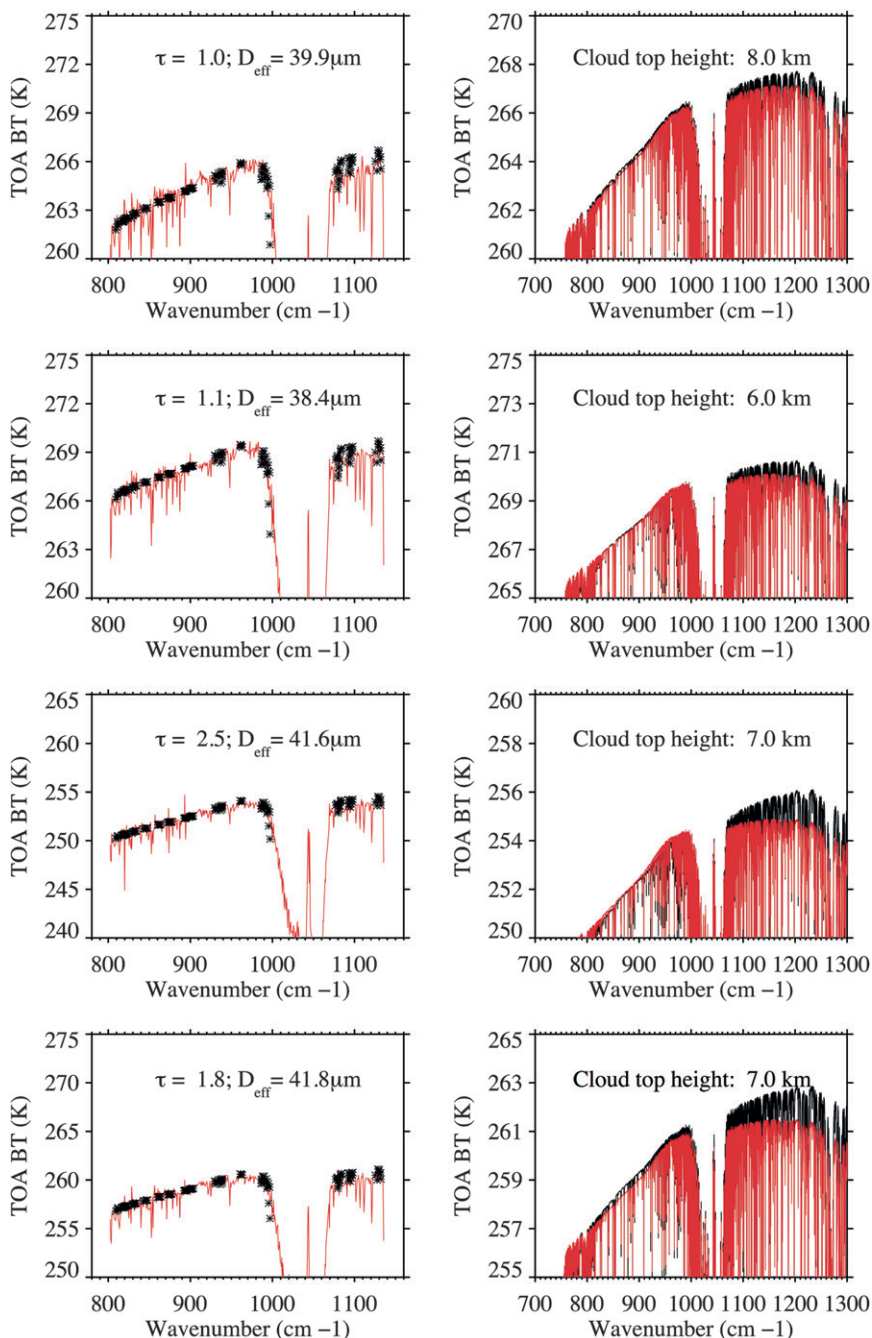


FIG. 11. (left) As in Fig. 10, but the cloud properties are retrieved according to the retrieval flowchart shown in Fig. 6. (right) Comparisons of TOA BT spectrum images given by different retrieval algorithms (red, after cloud-top altitude adjustment; black, using the MODIS cloud-top altitude).

radiance observations. This IR retrieval method simultaneously fits model-simulated and AIRS measurements from 800 to 960  $\text{cm}^{-1}$  and also minimizes BT differences between 985 and 1135  $\text{cm}^{-1}$  by selecting different  $\tau$ - $D_{\text{eff}}$  pairs and optimally adjusting the cloud-top height. The

differences between MODIS C5 operational retrievals and AIRS retrievals suggest that the solar channel method used in the MODIS C5 operational retrievals tends to result in larger  $\tau$  values than the IR retrieval. For the retrieved  $D_{\text{eff}}$  values, the IR method results in

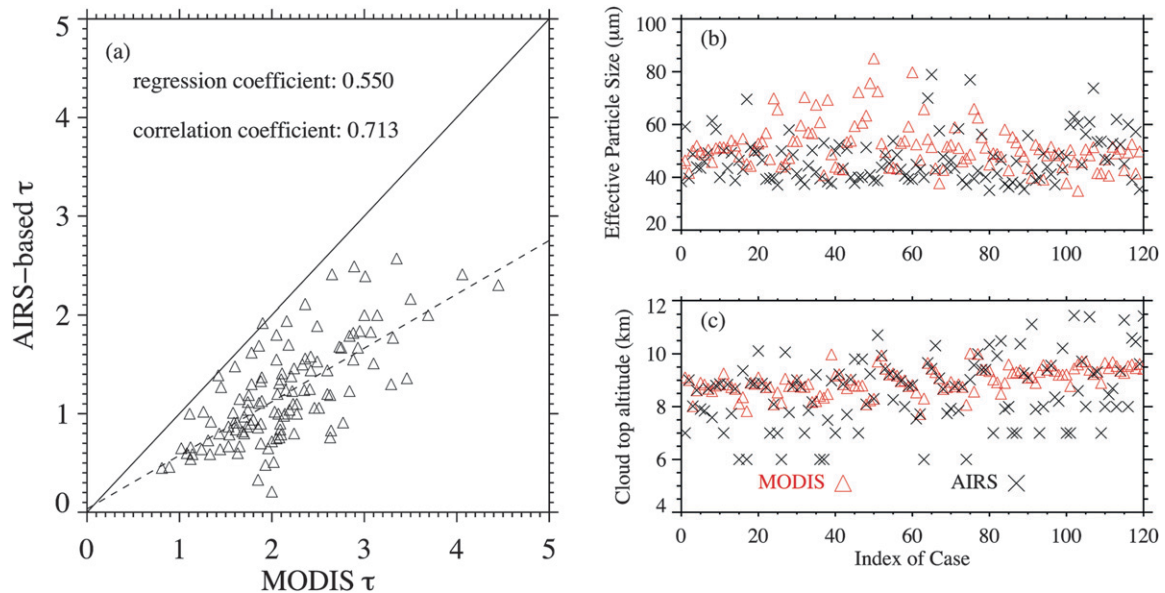


FIG. 12. Comparisons between IR-retrieved (a)  $\tau$ , (b)  $D_{\text{eff}}$ , and (c) cloud-top altitude with the MODIS C5 operational products.

slightly larger values over a wider range than do the MODIS C5 results. We investigate the discrepancies between MODIS C5 cloud-top height and those from the AIRS retrievals for the limited results in the case study. The comparisons indicate that about 50% of the MODIS-retrieved cloud-top heights need to be decreased by 1 km, and only 6% of them need to increase by 1 km. The cloud-height adjustment is necessary to minimize the differences between simulated and observed BTs.

Comparison of  $\tau$  values between the MODIS C5 product and the IR retrievals shows that the MODIS  $\tau$  values are systematically larger than their IR retrieved counterparts. Compared with the IR retrieval, the VIS–NIR-based retrieval is more sensitive to ice crystal shape (including particle surface roughness), cloud 3D effects, cloud inhomogeneity, and solar–satellite geometry. For instance, the current MODIS C5 ice cloud bulk scattering model assumes smooth and solid (bubble free) ice crystals. Some recent studies, however, have shown that the use of ice crystals with roughened surfaces (Baum et al. 2011) or with air bubbles (Xie et al. 2009) decreases the forward scattered energy and increases the backward energy (i.e., the asymmetry factor “ $g$ ” decreases). Passive radiance spaceborne sensors generally measure side- or backward scattered energy. To match a simulated reflectance to a given satellite-observed cloud reflectance, a larger  $\tau$  is required if  $g$  of the ice cloud is large. However, in the IR region,  $g$  is not sensitive to the particle shape and surface roughness. The best way to address the inconsistency between the IR and VIS–NIR cloud retrievals remains open. Some other requirements, such as a realistic ice cloud microphysical parameterization

scheme, accurate single-scattering properties of ice crystals, and a rigorous three-dimensional RTM, are necessary to improve our understanding.

*Acknowledgments.* This study was partly supported by NASA Grant NNX11AK37G, for which the principal investigator (PI) is Dr. Ping Yang; a subcontract (Contract 301K630) issued by the University of Wisconsin to Texas A&M University associated with a NASA grant (NNX11AF40G), for which the PI is Dr. Bryan Baum and the coinvestigators are Dr. Ping Yang and Dr. Andrew Heymsfield; and the endowment funds related to the David Bullock Harris Chair in Geosciences at the College of Geosciences, Texas A&M University. The Texas A&M Supercomputing Facility (<http://sc.tamu.edu/>) provides computational resources for the research reported in this paper.

## REFERENCES

- Arking, A., and K. Grossman, 1972: The influence of line shape and band structure on temperatures in planetary atmospheres. *J. Atmos. Sci.*, **29**, 937–949.
- Armbruster, W., and J. Fischer, 1996: Improved method of exponential sum fitting of transmissions to describe the absorption of atmospheric gases. *Appl. Opt.*, **35**, 1931–1941.
- Aumann, H. H., and Coauthors, 2003: AIRS/AMSU/HSB on the *Aqua* mission: Design, science objectives, data products, and processing systems. *IEEE Trans. Geosci. Remote Sens.*, **41**, 253–264.
- Baran, A. J., 2005: The dependence of cirrus infrared radiative properties on ice crystal geometry and shape of the size-distribution function. *Quart. J. Roy. Meteor. Soc.*, **131**, 1129–1142.

- , and P. N. Francis, 2004: On the radiative properties of cirrus cloud at solar and thermal wavelengths: A test of model consistency using high-resolution airborne radiance measurements. *Quart. J. Roy. Meteor. Soc.*, **130**, 763–778.
- Baum, B. A., A. J. Heymsfield, P. Yang, and S. T. Bedka, 2005: Bulk scattering properties for the remote sensing of ice clouds. Part I: Microphysical data and models. *J. Appl. Meteor.*, **44**, 1885–1895.
- , P. Yang, S. L. Nasiri, A. K. Heidinger, A. J. Heymsfield, and J. Li, 2007: Bulk scattering properties for the remote sensing of ice clouds. Part III: High-resolution spectral models from 100 to 3250  $\text{cm}^{-1}$ . *J. Appl. Meteor. Climatol.*, **46**, 423–434.
- , —, A. J. Heymsfield, C. G. Schmitt, Y. Xie, A. Bansemmer, Y. Hu, and Z. Zhang, 2011: Improvements in shortwave bulk scattering and absorption models for the remote sensing of ice clouds. *J. Appl. Meteor. Climatol.*, **50**, 1037–1056.
- Blumstein, D., and Coauthors, 2004: IASI instrument: Technical overview and measured performances. *Infrared Spaceborne Remote Sensing XII*, M. Strojnik, Ed., International Society for Optical Engineering (SPIE Proceedings, Vol. 5543), 196–207.
- Clough, S. A., F. X. Kneizys, and R. W. Davies, 1989: Line shape and the water vapor continuum. *Atmos. Res.*, **23**, 229–241.
- , M. W. Shephard, E. J. Mlawer, J. S. Delamere, M. J. Iacono, K. Cady-Pereira, S. Boukabara, and P. D. Brown, 2005: Atmospheric radiative transfer modeling: A summary of the AER codes. *J. Quant. Spectrosc. Radiat. Transfer*, **91**, 233–244.
- Cooper, S. J., and T. J. Garrett, 2010: Identification of small ice cloud particles using passive radiometric observations. *J. Appl. Meteor. Climatol.*, **49**, 2334–2347.
- DeSlover, D. H., W. H. Smith, P. Piironen, and E. W. Eloranta, 1999: A methodology for measuring cirrus cloud visible to infrared spectral optical depth ratios. *J. Atmos. Oceanic Technol.*, **16**, 251–262.
- Dubuisson, P., V. Giraud, O. Chomette, H. Chepfer, and J. Pelon, 2005: Fast radiative transfer modeling for infrared imaging radiometry. *J. Quant. Spectrosc. Radiat. Transfer*, **95**, 201–220.
- Eguchi, N., T. Yokota, and G. Inoue, 2007: Characteristics of cirrus clouds from ICESat/GLAS observations. *Geophys. Res. Lett.*, **34**, L09810, doi:10.1029/2007GL029529.
- Gallery, W. O., F. X. Kneizys, and S. A. Clough, 1983: Air mass computer program for atmospheric transmittance/radiance calculations: FSCATM. Air Force Geophys. Laboratory Rep. AFGL-TR-83-0065, Hanscom AFB, MA, 145 pp. [NTIS ADA-175173.]
- Goody, R., R. West, L. Chen, and D. Crisp, 1989: The correlated-k method for radiation calculations in nonhomogeneous atmospheres. *J. Quant. Spectrosc. Radiat. Transfer*, **42**, 539–550.
- Hansen, J. E., and J. W. Hovenier, 1971: The doubling method applied to multiple scattering of polarized light. *J. Quant. Spectrosc. Radiat. Transfer*, **11**, 809–812.
- Hartmann, D. L., and D. A. Short, 1980: On the use of earth radiation budget statistics for studies of clouds and climate. *J. Atmos. Sci.*, **37**, 1233–1250.
- Heidinger, A. K., C. O'Dell, R. Bennartz, and T. Greenwald, 2006: The successive-order-of-interaction radiative transfer model. Part I: Model development. *J. Appl. Meteor. Climatol.*, **45**, 1388–1402.
- Herman, G. F., M. C. Wu, and W. T. Johnson, 1980: The effect of clouds on the earth's solar and infrared radiation budgets. *J. Atmos. Sci.*, **37**, 1251–1261.
- Heymsfield, A. J., and J. Iaquinta, 2000: Cirrus crystal terminal velocities. *J. Atmos. Sci.*, **57**, 916–938.
- , A. Bansemmer, P. R. Field, S. L. Durden, J. L. Stith, J. E. Dye, W. Hall, and C. A. Grainger, 2002: Observations and parameterizations of particle size distributions in deep tropical cirrus and stratiform precipitating clouds: Results from in situ observations in TRMM field campaigns. *J. Atmos. Sci.*, **59**, 3457–3491.
- Huang, H.-L., P. Yang, H. Wei, B. A. Baum, Y.-X. Hu, P. Antonelli, and S. A. Ackerman, 2004: Inference of ice cloud properties from high-spectral resolution infrared observations. *IEEE Trans. Geosci. Remote Sens.*, **42**, 842–852.
- Huang, X. L., Y. L. Yung, and J. S. Margolis, 2003: Use of high-resolution measurements for the retrieval of temperature and gas concentration profiles from outgoing infrared spectra in the presence of cirrus clouds. *Appl. Opt.*, **42**, 2155–2165.
- Kahn, B. H., and Coauthors, 2003: Near micron-sized cirrus cloud particles in high-resolution infrared spectra: An orographic case study. *Geophys. Res. Lett.*, **30**, 1441, doi:10.1029/2003GL016909.
- , A. Eldering, M. Ghil, S. Bordoni, and S. A. Clough, 2004: Sensitivity analysis of cirrus cloud properties from high-resolution infrared spectra. Part I: Methodology and synthetic cirrus. *J. Climate*, **17**, 4856–4870.
- Kratz, D. P., 1995: The correlated k-distribution technique as applied to the AVHRR channels. *J. Quant. Spectrosc. Radiat. Transfer*, **53**, 501–517.
- Lacis, A., and V. Oinas, 1991: A description of the correlated k distribution method for modeling nongray gaseous absorption, thermal emission, and multiple scattering in vertically inhomogeneous atmospheres. *J. Geophys. Res.*, **96**, 9027–9063.
- , W. C. Wang, and J. Hansen, 1979: Correlated k-distribution method for radiative transfer in climate models: Application to effect of cirrus clouds on climate. *NASA Conf. Publ.*, **2076**, 309–314.
- Li, J., W. P. Menzel, W. Zhang, F. Sun, T. J. Schmit, J. Gurka, and E. Weisz, 2004: Synergistic use of MODIS and AIRS in a variational retrieval of cloud parameters. *J. Appl. Meteor.*, **43**, 1619–1634.
- Liu, X., W. L. Smith, D. K. Zhou, and A. Larar, 2006: Principal component-based radiative transfer model for hyperspectral sensors. *Appl. Opt.*, **45**, 201–209.
- McFarquhar, G. M., A. J. Heymsfield, J. Spinhirne, and B. Hart, 2000: Thin and subvisual tropopause tropical cirrus: Observations and radiative impacts. *J. Atmos. Sci.*, **57**, 1841–1853.
- Mlawer, E. J., S. A. Clough, and D. C. Tobin, 2003: The MT\_CKD water vapor continuum: A revised perspective including collision induced effects. *Proc. 10th Conf. on Atmospheric Science from Space using Fourier Transform Spectrometry*, Bad Wildbad, Germany, Institut für Meteorologie und Klimaforschung. [Available online at [http://www-imk.fzk.de/asf/ame/ClosedProjects/assfts/O\\_I\\_7\\_Clough\\_SA.pdf](http://www-imk.fzk.de/asf/ame/ClosedProjects/assfts/O_I_7_Clough_SA.pdf).]
- Moncet, J. L., G. Uymin, A. E. Lipton, and H. E. Snell, 2008: Infrared radiance modeling by optimal spectral sampling. *J. Atmos. Sci.*, **65**, 3917–3934.
- Nakajima, T., and M. D. King, 1990: Determination of the optical thickness and effective particle radius of clouds from reflected solar radiation measurements. Part I: Theory. *J. Atmos. Sci.*, **47**, 1878–1893.
- Niu, Y., P. Yang, H. L. Huang, J. E. Davies, J. Li, B. A. Baum, and Y. X. Hu, 2007: A fast infrared radiative transfer model for overlapping clouds. *J. Quant. Spectrosc. Radiat. Transfer*, **103**, 447–459.

- Ohring, G., and P. Clapp, 1980: The effect of changes in cloud amount on the net radiation at the top of the atmosphere. *J. Atmos. Sci.*, **37**, 447–454.
- Rienecker, M. M., and Coauthors, 2008: The GEOS-5 data assimilation system—Documentation of versions 5.0.1, 5.1.0, and 5.2.0. NASA Tech. Rep. Series on Global Modeling and Data Assimilation 27, NASA/TM-2008-104606, 1–118. [Available online at <http://gmao.gsfc.nasa.gov/pubs/docs/Rienecker369.pdf>.]
- Rothman, L. S., and Coauthors, 2005: The HITRAN 2004 molecular spectroscopic database. *J. Quant. Spectrosc. Radiat. Transfer*, **96**, 139–204.
- Saunders, R., M. Matricardi, and P. Brunel, 1999: An improved fast radiative transfer model for assimilation of satellite radiance observations. *Quart. J. Roy. Meteor. Soc.*, **125**, 1407–1425.
- , P. Brunel, S. English, P. Bauer, U. O’Keeffe, P. Francis, and P. Rayer, 2006: RTTOV-8—Science and validation report. Met Office Forecasting and Research Tech. Doc. NWPSAF-MO-TV-007, 46 pp.
- Stamnes, K., S. C. Tsay, W. Wiscombe, and K. Jayaweera, 1988: Numerically stable algorithm for discrete-ordinate-method. *Appl. Opt.*, **27**, 2502–2509.
- Stephens, G. L., 2005: Cloud feedbacks in the climate system: A critical review. *J. Climate*, **18**, 237–273.
- Tobin, D. C., H. E. Revercomb, C. C. Moeller, and T. S. Pagano, 2006: Use of atmospheric infrared sounder high-spectral resolution spectra to assess the calibration of Moderate Resolution Imaging Spectroradiometer on EOS Aqua. *J. Geophys. Res.*, **111**, D09S05, doi:10.1029/2005JD006095.
- Twomey, S., N. Jacobowitz, and H. B. Howell, 1966: Matrix methods for multiple-scattering problems. *J. Atmos. Sci.*, **23**, 289–296.
- Wang, C., P. Yang, B. A. Baum, S. Platnick, A. K. Heidinger, Y. X. Hu, and R. E. Holz, 2011: Retrieval of ice cloud optical thickness and effective particle size using a fast infrared radiative transfer model. *J. Appl. Meteor. Climatol.*, **50**, 2283–2297.
- Wei, H., P. Yang, J. Li, B. A. Baum, H. L. Huang, S. Platnick, Y. X. Hu, and L. Strow, 2004: Retrieval of semitransparent ice cloud optical thickness from Atmospheric Infrared Sounder (AIRS) measurements. *IEEE Trans. Geosci. Remote Sens.*, **42**, 2254–2266.
- , X. Chen, R. Rao, Y. Wang, and P. Yang, 2007: A moderate-spectral-resolution transmittance model based on fitting the line-by-line calculation. *Opt. Express*, **15**, 8360–8370.
- Wiscombe, W. J., and J. W. Evans, 1997: Exponential-sum fitting of radiative transmission functions. *J. Comput. Phys.*, **24**, 416–444.
- Xie, Y., P. Yang, G. W. Kattawar, P. Minnis, and Y. X. Hu, 2009: Effect of the inhomogeneity of the ice crystals on retrieving ice cloud optical thickness and effective particle size. *J. Geophys. Res.*, **114**, D11203, doi:10.1029/2008JD011216.
- Yang, P., H. Wei, H. L. Huang, B. A. Baum, Y. X. Hu, G. W. Kattawar, M. I. Mishchenko, and Q. Fu, 2005: Scattering and absorption property database for nonspherical ice particles in the near-through far-infrared spectral region. *Appl. Opt.*, **44**, 5512–5523.
- Yue, Q., and K. N. Liou, 2009: Cirrus cloud optical and microphysical properties determined from AIRS infrared spectra. *Geophys. Res. Lett.*, **36**, L05810, doi:10.1029/2008GL036502679.
- , —, and S. C. Ou, 2007: Interpretation of AIRS data in thin cirrus atmospheres based on a fast radiative transfer model. *J. Atmos. Sci.*, **64**, 3827–3842.
- Zhang, Z., and Coauthors, 2004: Geometric optics solution to light scattering by droxtal ice crystals. *Appl. Opt.*, **43**, 2490–2499.
- , and Coauthors, 2007: A fast infrared radiative transfer model based on the adding-doubling method for hyperspectral remote-sensing applications. *J. Quant. Spectrosc. Radiat. Transfer*, **105**, 243–263.
- , P. Yang, G. W. Kattawar, J. Riedi, L.-C. Labonnote, B. A. Baum, S. Platnick, and H. L. Huang, 2009: Influence of ice particle model on satellite ice cloud retrieval: Lessons learned from MODIS and POLDER cloud product comparison. *Atmos. Chem. Phys.*, **9**, 7115–7129.
- , S. Platnick, P. Yang, A. K. Heidinger, and J. M. Comstock, 2010: Effects of ice particle size vertical inhomogeneity on the passive remote sensing of ice clouds. *J. Geophys. Res.*, **115**, D17203, doi:10.1029/2010JD013835.